ACS APPLIED MATERIALS & INTERFACES
Research Article
www.acsami.org

Large Area IR Microlens Arrays of Chalcogenide Glass Photoresists by Grayscale Maskless Lithography

Yogeenth Kumaresan, Amritha Rammohan, Prabhat K. Dwivedi, and Ashutosh Sharma*

Department of Chemical Engineering, Indian Institute of Technology Kanpur, Kanpur 208016, India

ABSTRACT: The ability to use chalcogenide glass thin films as photoresists for one-step maskless grayscale lithographic patterning is demonstrated. It is shown that the chalcogenide photoresists can be used to fabricate grayscale patterns with smooth and continuous profiles such as arrays of cylindrical and spherical microlenses, which are useful as optical structures for IR applications. The etching and exposure parameters are optimized to obtain smooth reproducible lens arrays of 150 μm periodicity and up to ~170 nm height on large areas (~1 cm^2). The roughness is found to increase as a function of the exposure dose and is attributed to the selective dissolution of the As−Se, As−As, and Se−Se bonds present in the nanodistributed phases and the presence of the oxide phase. Thus, a minimum exposure dose produces optimally patterned lens arrays. The focal length calculated for the smooth microlens array is ~9.3 mm, indicating the suitability of the lens arrays for focusing applications in the IR region.

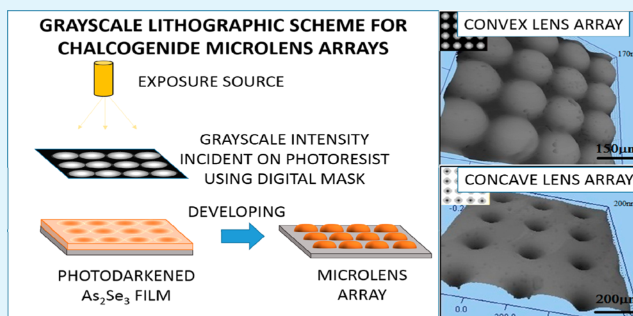

KEYWORDS: *chalcogenide glass, thin film, grayscale lithography, microlens arrays, photopatterning, maskless lithography*

1. INTRODUCTION

Chalcogenide glasses have become promising materials for a variety of infrared optics (IR) applications based on the photoinduced effects that these materials exhibit.[1−5] One of the most interesting of these properties is the change in the chemical resistance to various solvents on exposure to light of appropriate wavelength and intensity.[6,7] This property allows the use of these materials as inorganic photoresists in photolithography. Chalcogenide photoresists have several advantages over polymer-based organic photoresists because of their smaller fundamental structural units and strong covalent bonds that makes lithographic patterning of small and robust 3D features possible.[8,9] Deposition of chalcogenide glasses over large homogeneous areas with a low concentration of chemical inhomogeneities is also achievable by techniques such as thermal evaporation and sputtering.[10] It is also important to note that the pre-baking and post-baking steps of polymer photoresist-based lithography are also eliminated. Photoresist properties together with high transmission in the IR region are advantageous for creating microlens arrays and optical gratings for application in medical tomography, optical communication, CCD cameras, and microimaging systems.[10−12] These periodic lens arrays also have a reduced depth of focus as compared to a single lens and can thus reduce device size when employed in micro-optical devices.[13] However, the widespread use of these structures requires a reliable and high-resolution fabrication technique to reproducibly construct high quality defect-free 3D structures. The main techniques for fabricating microlens arrays are based on chalcogenide photoresists such as As_2S_3, As_2Se_3, $Ge_{10}Se_{50}As_{40}$, and $As_{10}S_{60}Ge_{30}$.[1,14−16] They have been used as negative or positive type inorganic photoresists based on the specific solvent used as the developer.[8] However, for fabrication of truly curved and optically smooth structures such as lenses, the conventional planar or 2D techniques of lithography are not suitable. Thus, fabrication of microlens arrays in these materials requires novel adaptations of lithographic techniques.

Eisenberg and co-workers have developed various lithographic techniques for the fabrication of 3D structures in chalcogenide photoresists such as proximity lithography, grayscale mask lithography, and thermal reflow.[15−18] In the proximity method, one major limitation inherent to the technique is the low fill factor of the microlens due to the lateral spreading of the light. In the thermal reflow method, fabricated microlenses are required to be transferred on a suitable substrate by using anisotropic etching. However, many parameters have to be optimized in anisotropic etching to get the desired pattern. Halftone or continuous tone grayscale mask lithography used by Eisenberg et al.[19] involves the use of a physical grayscale mask having a light transmission gradient, which is usually fabricated by expensive techniques. This mask is then used in the contact mode to directly fabricate a designed shape in chalcogenide photoresists. Other techniques used to create optical elements using chalcogenides include soft lithography,[20] holographic techniques,[21] and interference

Received: April 17, 2013
Accepted: July 5, 2013
Published: July 24, 2013

© 2013 American Chemical Society

dx.doi.org/10.1021/am401368e | ACS Appl. Mater. Interfaces 2013, 5, 7094−7100

photolithography,[22,23] etc., which involve multiple or complicated steps or expensive equipments.

Recently, Kovalskiy et al.[14] have used high-energy beam-sensitive (HEBS) blank glass masks created by e-beam lithography for fabrication of the lens arrays. They used these masks along with a mask aligner to expose thermally deposited As−S thin films followed by wet and dry negative etching processes. It was found that surface roughness of the dry etched fabricated structures is undesirably high. The fabrication of the HEBS mask and exposure by e-beam are time-consuming processes, especially for thicker films. As compared to e-beam or other serial writing techniques, a parallel technique where the entire substrate is exposed at once is more advantageous.

We have previously demonstrated a grayscale maskless lithographic technique for the fabrication of 3D structures in a SU-8 photoresist in a single lithographic step.[24] We demonstrate here the application of grayscale maskless lithography to a chalcogenide photoresist for the facile fabrication of 3D microlens arrays in a single lithographic step. Here, the light intensity incident on the photoresist is scaled by a grayscale value that ranges from 0 (black) to 255 (white) on a digital image file. This grayscale value is translated into variation in light intensity incident on a photoresist through a digital micromirror device (DMD) consisting of an array of micromirrors that can be rapidly reconfigured by software and can pattern over an area of ∼1 cm^2.[24] An intermediate exposure intensity in proportion to the grayscale value is obtained by controlling the ratio of the time a micromirror reflects UV light onto the photoresist to the total time of exposure. The $x-y$ patterning is achieved by creating computer generated images with regions varying in grayscale value. We thus demonstrate patterning of chalcogenide photoresists thin films in a single lithographic step by using the grayscale capabilities of the maskless exposure system. Further, we explore the mechanism responsible for the creation of roughness and optimize the lithographic parameters such as the developer, developing time, and exposure dose to obtain relatively smooth and truly curved reproducible periodic structures such as convex and concave microlens arrays in a single lithographic step.

2. EXPERIMENTAL PROCEDURE

Amorphous thin films of $As_{40}Se_{60}$ with various thicknesses (∼0.2−2.0 μm) were prepared from commercially available bulk chalcogenide glasses obtained from VITRON GmbH, Germany. Films were prepared by thermal evaporation (HHV, India, model 12A4D-T) onto rotating substrates at room temperature. Precleaned microscopic glass slides (RivieraTM, India) and silicon wafers (Wafer World, Inc., U.S.A.) were used as substrates. The glass slides and Si wafers were cut into approximately 1 in. × 1 in. squares prior to deposition. The deposition rate of the films in a vacuum of 2×10^{-6} Torr was controlled to ∼10 nm/s. The substrate holder was rotated at frequency ∼3 Hz during the deposition to produce uniform films of 2 μm thickness. The films were annealed for 2 h at 150 °C for stabilizing the films prior to conducting exposure experiments.

The field emission scanning electron microscope (Carl Zeiss, Supra 40 VP) and attached energy dispersive X-ray analyzer (Oxford, U.K.; spatial resolution 0.5 μm radius) were used to confirm the homogeneity of surface topography and the chemical composition on different spots of the films. The data over six points were averaged for surface composition across the film. Confocal Raman spectroscopy (Witec) was used to observe the chemical homogeneity across the depth of the films. The amorphous nature of the films was checked by means of the X-ray diffraction measurements (PAN alytical, The Netherlands). All the samples were stored in complete darkness and in a clean and moisture-free, glovebox (VAC, U.S.A.) environment to prevent them from possible oxidation and/or exposure. The annealed chalcogenide samples were cleaned with nitrogen blowing and were heated to 50 °C to remove adsorbed moisture prior to exposure. The UV irradiation of the films was done in clean room environment (Class 100) by mercury lamp (power density ∼15 mW/cm^2) attached to a maskless lithography system (SF-100 from Intelligent Micro patterning LLC, St. Petersburg, FL). The grayscale software mask was designed in Microsoft bitmap software. The power density of the mercury lamp was measured with a UV power meter (model 306, OAI, U.S.A.). The exposure setup was calibrated such that each pixel in the electronic file corresponded to an area of 15 μm^2 on the photoresist substrate. The exposure light intensity is given by the RGB (red, green, and blue) code of the color used to fill a specific pattern. A reproducible grayscale was implemented by setting the red, green, and blue all to the same value between 0 and 255 (0 for black and 255 for white). The grayscale software mask was prepared by varying the value between 0 and 255 in order to obtain the curve shaped structure. Exposure time used for the samples was varied from 900 to 3600 s with lamp power density measured at 15 mW/cm^2 for blank white light. The dose delivered to each 15 μm^2 area of the sample is a function of the grayscale RGB value of the corresponding pixel and exposure time. Lens arrays of more than 4000 lenses over an area of 1 cm^2 could be exposed on the As_2Se_3 thin film.

Exposed films were developed in different amine-based developers ethanolamine, butylamine, and propylamine (Fisher Scientific, India) in a glass beaker for up to 3 min with constant agitation. After development, the samples were rinsed in IPA (isopropyl alcohol, Fisher Scientific, India) and dried using a nitrogen gun. For dissolution kinetics, the difference in height between the exposed and unexposed region was plotted as etch depth. All samples were analyzed using both an optical microscope (Leica, DM 2500 M) and field emission scanning electron microscope (FESEM). Surface profiling of the fabricated lens structure was carried out using an optical profiling system (NanoMap-D, Aep Technlogy, U.S.A.) and the thicknesses of the developed films were characterized using an atomic force microscope (AFM) from Agilent PICOSPM II.

3. RESULTS AND DISCUSSION

3.1. Characterization of As-Deposited and Annealed Films. The chemical composition and distribution of phases in the as-deposited and annealed films were characterized before subjecting to lithographic treatment. This can serve as the reference to understand the effect of grayscale exposure on the chemical properties of the As_2Se_3 films. The chemical composition of the as-deposited films was analyzed by EDAX (energy dispersive X-ray analysis) measurements at different points on the surface of the film. The data averaged across six points showed an over stoichiometric amount of As (41.4 at % in film as compared to bulk 40 at %) and substoichiometric amount of Se (films: Se 58.2 at %, bulk 60 at %) possibly due to the higher volatility of selenium as compared to the arsenic.[25] A negligible amount of oxygen was observed on the surface by EDAX. The chemical nature of the films was previously analyzed by us using Raman spectra measurements.[26] The As−As, Se−Se, and As−Se bond peaks and peaks arising from Se rings, etc. were confirmed. In addition, we have also found that the peaks observed using confocal Raman spectroscopy at different depths of a single film appear to be constant indicating chemical homogeneity across the depth of the 2 μm thick film. Furthermore, the amorphous nature of the annealed films was also confirmed by the absence of sharp peaks in the XRD graph (results not shown).

3.2. Grayscale Lithographic Scheme. Chalcogenide thin films undergo photostructural changes when exposed to UV light. Exposed areas of the films are selectively protected from

the etchant in proportion to the irradiation dose as is the case with all negative photoresists. Grayscale lithography is based on the fact that not only the exposure time but the light intensity also affects the selective protection. Figure 1 shows a scheme of

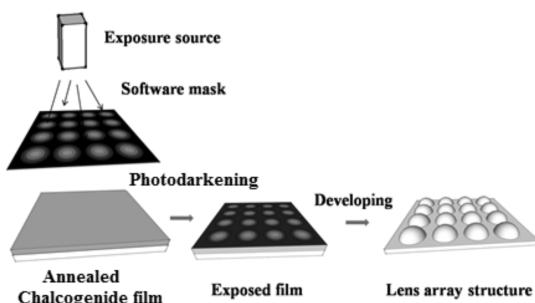

Figure 1. Schematic of grayscale lithography for As_2Se_3 chalcogenide photoresist.

the grayscale lithography for the patterning of convex spherical lens arrays in chalcogenide glasses. The first step is the designing of a suitable digital mask for lenses. Considering the process for a negative photoresist, thicker regions are created by having corresponding regions in the digital mask that transmit more light, and thinner regions are created by having regions that transmit less light in the mask. This graded exposure causes photoinduced changes that affect the structure and ordering of the chalcogenide film.[27] The desired micropattern is obtained by developing with a suitable selective solvent.

Another effect of the exposure of chalcogenides to light is the photo expansion effect, i.e., the increase in dimensions on exposure to light. Various researchers have encountered this phenomenon. Tanaka et al.[28] found a photo expansion of an ~5% increase in the As_2S_3 flake of thickness 50 μm by irradiating with a 632.82 nm He−Ne laser and focusing a 2.0 eV light of 103 W/cm^2 intensity. Bishop and co-workers[29] have also reported a photo expansion as high as 10% of the irradiated volume using 514 nm light (photo energy = 2.41 eV) from an Argon iron laser. Photo expansion in these disks of As_2S_3 depends on the source and intensity used for irradiation. In our case, a lamp (i line 365 nm, g line 436 nm) having maximum 15 mW/cm^2 power density was used for exposure with a grayscale mask to minimize the photoexpansion effect. To verify this, we exposed one part of the annealed film using a UV light source for the maximum time (3600 s) and covered other part with Teflon to avoid exposure. After exposure, we measured the height difference between two regions (exposed and unexposed) using an optical profilometer. The height difference between two regions was found to be of negligible magnitude. Thus, under the exposure conditions employed in all the experiments, a negligible photo expansion is to be expected.

3.3. Grayscale Lithography: Effects of Developing Solution and Developing Time. A suitable developer can be chosen based on many criteria such as safety of use, defect-free etching, selectivity, etc. However, for grayscale lithography, a sensitive developer is required to proportionally etch regions exposed with closely varying grayscale intensity values. A greater range of profile heights can thus be patterned. The sensitivity of a developer is characterized by the ratio of the rates of etching of exposed and unexposed areas. Furthermore, if a developer with fast dissolution kinetics is used, then the etch profile is not determined by the developing parameters. Instead, it is predominantly a function of the exposure intensity or the grayscale value at a region alone.

To find an optimal developer for grayscale lithography, we considered three primary amines: ethanolamine, propylamine, and butylamine. Manevich et al.[18] and Bryce et al.[10] have already reported amines as a good negative etchants for As_2Se_3. The mechanism of selective etching of exposed and unexposed regions is due to the differential etching of homopolar and heteropolar bonds in the As_2Se_3 films. Regions exposed to UV have been found to have a higher concentration of heteropolar bonds of the As−Se type that are more resistant to etching by amine developers. Hence, amine developers with As_2Se_3 films create the negative photoresist combination.[30,31] To understand the dissolution kinetics of the three developers, we exposed annealed As_2Se_3 films to white exposure for 1800 s and developed each of the samples in a different developer solution. The etch depth was measured by optical profilometry at regular intervals as shown in Figure 2. From the graph, it is apparent

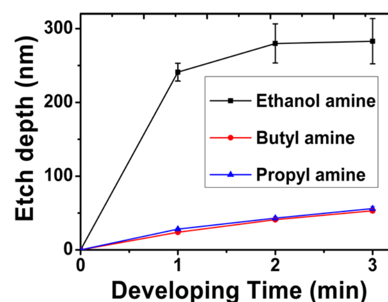

Figure 2. Etch depth variation with increasing developing time in ethanolamine, propylamine, and butylamine.

that after 3 min, the saturation etch depth is reached for the case of ethanol amine, while the etch depth in the case of butyl and propyl amine shows a linearly increasing trend. Thus, in the case of ethanol amine, we can expect the saturation depth at each grayscale value to be reached within 3 min and not vary as a function of the developing time. On the other hand, in the case of propyl and butyl amine, it takes a longer time for saturation depth to be reached, and hence, the etch profile depends on the developing time as well as grayscale intensity of exposure.

This difference in dissolution kinetics across the different primary amines is due to the difference in polarity of the solvent.[30−32] Butylamine being the strongest base has the lowest polarity, while ethanolamine has the highest polarity among the three primary amines. Thus, the dissolution reaction involving ethanolamine is fastest among the three solvents. In further experiments, ethanol amine was used as the developer.

Next, to understand the sensitivity of the developer to the exposed and unexposed regions, we exposed an annealed As_2Se_3 film to blank (white) exposure for 900 s. The exposed film and a control unexposed film were then developed in ethanolamine. Their etch depths were measured using optical profilometry at regular intervals as shown in Figure 3. As expected, the etch depth of unexposed film decreases faster than that of the exposed film. The complete dissolution of an unexposed region of an ~800 nm height takes around 3 min. Also, the maximum difference in the height between the exposed and unexposed etch depths is also at ~3 min. Hence, a developing time of 3 min is found to be the optimum developing time for the As_2Se_3 films.

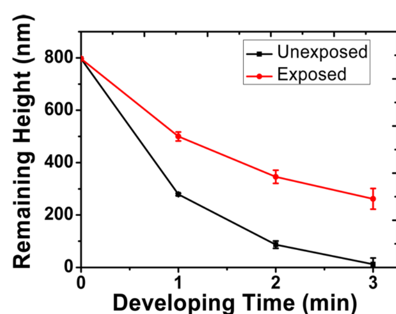

Figure 3. Remaining height as a function of developing time for exposed and unexposed regions of a sample exposed for 900 s in ethanolamine.

3.4. Grayscale Lithography: Effect of Exposure Dose.

After the developer and developing time were fixed to their near optimal values, the effect of exposure dose, i.e., exposure intensity or grayscale value and exposure time, was analyzed. In the first set of experiments, four different As_2Se_3 thin films with thickness of ~2 μm were exposed for 900, 1800, 2700, and 3600 s with blank white exposure. The films were then developed in ethanolamine for 3 min according to our previously optimized developing parameters. The heights of the films were measured using AFM and are plotted in Figure 4 as a function of exposure time. We note from the result that the height of the film after developing is roughly proportional to the exposure time. An exposure time of 3600 s was sufficient to obtain 700 nm high films. While a higher exposure time would result in taller structures, we expect that defects would increase. Exposure systems usually also have limitations of maximum continuous exposure for maintaining stable light intensities. Hence, we have used a maximum exposure time of 3600 s.

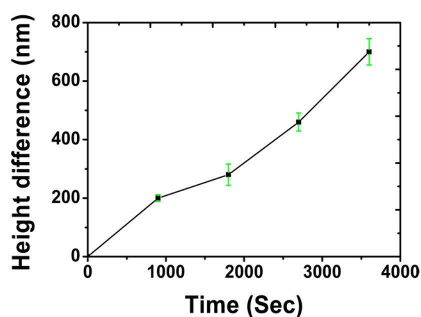

Figure 4. Height difference between exposed and unexposed regions after 3 min of developing in ethanol amine plotted as a function of exposure time. Height difference was measured using an AFM.

Using the limit of exposure time of 3600 s, as-deposited As_2Se_3 films were exposed using a grayscale pattern. A grayscale software mask was designed by areas of lighter grays (higher grayscale or RGB value) where a taller structure was desired and darker grays (lower grayscale value) where shorter structures were desired. Concave cylindrical lens arrays were fabricated by using alternating black and white strips with gradually varying grayscale values in between the two in the software mask as shown in the inset of Figure 5a. Figure 5a shows the Brightfield microscope image of an array of concave cylindrical microlenses exposed for 3600 s. Figure 5b shows the optical profilometer image of the cylindrical microlens array.

The profile clearly proves the grayscale patterning of chalcogenides by showing heights proportional to regions of grayscale. Regions with lighter grays are higher than regions of lower grayscale values with maximum values of 700 nm at the white regions. The profile also shows the regular and uniform periodic structures, indicating that the heights are reproducible with respect to the corresponding grayscale value. This means that once the lithographic parameters are fixed the etch depth or pattern height is a function only of the grayscale value, and this information can be extrapolated to any desirable structure. The profile also shows a relatively smooth curved structure without any digitization of height. This is due to the soft contrast characteristics in grayscale lithography of chalcogenides.[19] However, the surface roughness measured at the top surface of the lenses is undesirably high (~50 nm).

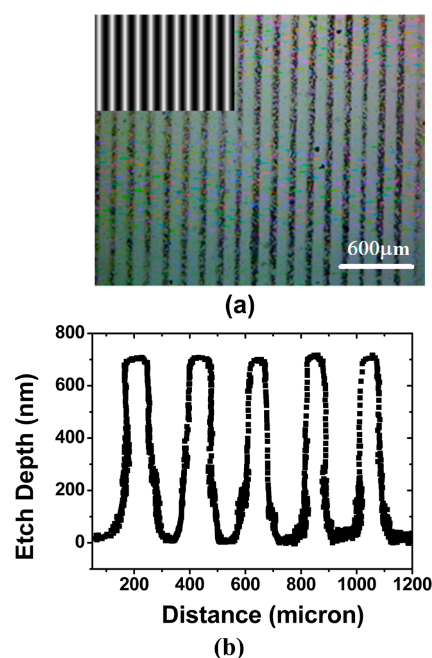

Figure 5. (a) Brightfield microscope image of fabricated array of cylindrical microlens arrays in As_2Se_3 (inset shows grayscale software mask used). (b) Profilogram demonstrating the change of height in the fabricated structures in As_2Se_3 with gradual variation of the grayscale mask. It may be noted that in (b) the x axis (nm) and y axis (micrometer) scales are vastly different resulting in compression of feature widths.

3.5. Origin of Roughness.

The drawback in using many chalcogenide patterning techniques for fabricating optical elements is the undesirably high roughness of the lenses making them less useful for optical applications.[7,33] To understand the origin of roughness in lenses patterned at 3600 s exposure, we characterized the surface of the as-deposited and annealed chalcogenide films. The roughness of the as-deposited and annealed films was measured by optical profilometer across more than one sample. The roughness of the as-deposited films was found to be ~5 ± 1 nm, and after annealing, the roughness decreased to ~2 ± 1 nm. This level of roughness indicates the relatively smooth nature of the annealed chalcogenide films before exposure. The reduction in roughness upon annealing is not significant enough to draw major conclusions. However, the change can possibly be attributed to the stabilization (i.e., polymerization of molecular units into the matrix reducing the number of homopolar bonds)[23] of the film and filling of voids created during the deposition process. Further, the AFM profiles of samples that

had both exposed and unexposed regions used in Section 3.4 were analyzed. The roughness in the unexposed and exposed regions of the films was measured at each exposure time and plotted (Figure 6). As is clear from the graph, the roughness

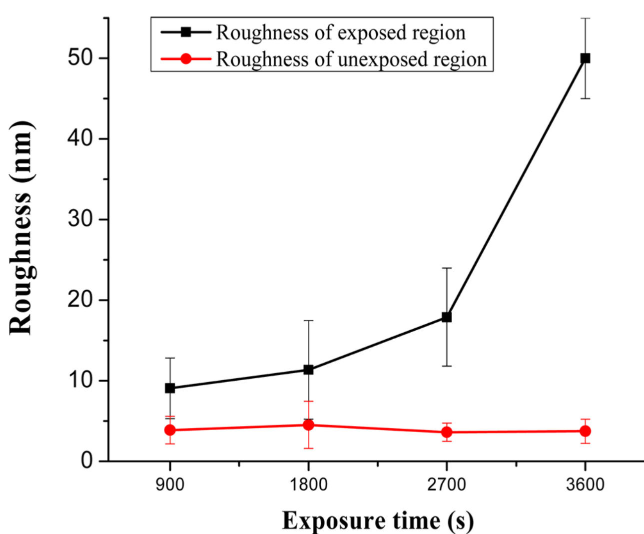

Figure 6. Plot of roughness after developing as a function of exposure time.

increases as a function of exposure time for exposed regions, while the roughness of unexposed regions stays more or less constant. From this one can conclude that the nanoscale roughness originates from the exposure step of lithographic patterning. However, certain bigger defects (>1 μm in diameter) are also observed. These defects can be attributed to the oxide phase As_2O_3 that arises on exposure of As_2Se_3 in the presence of oxygen[34] and can be potentially addressed by exposure in inert conditions.

The roughness variation with exposure time can be explained if we consider the chemical changes that occur upon exposure of the As_2Se_3 films to UV radiation. We have previously reported the chemical changes that occur in As_2Se_3 films on exposure to UV radiation using Raman spectra measurements. The homopolar bonds in the chalcogenides, namely, As−As and Se−Se, decrease with increasing the UV exposure time. However, the heteropolar bonds between As and Se increase. The selective etching of the unexposed areas arises from relatively higher rate of dissolution of the homopolar bonds in the developer.[14] The origin of roughness after chemical etching could be due to a difference in etching rates of As−As bonds and Se−Se bonds. A similar observation was found for As_2S_3 films that were plasma-etched by Choi and co-workers.[35] They have attributed the surface roughness in As_2S_3 films to the differential chemical attack of As- and S-rich phases in the thermally deposited films. Although their observations are in the case of plasma etching and for the As−S system, one can make a parallel argument considering the origin of roughness in the exposure step. In our case, As_2Se_3 film regions exposed to radiation contain $AsSe_3$ pyramids, As_4Se_3 units, and Se_8 rings. Each of these contain As−As bonds and Se−Se bonds in different proportions, thus creating As-rich phases and Se-rich phases. The differential etching of the As−As and Se−Se bonds implies a differential etching of the above phases, and the nanoscale distribution of the As-rich and Se-rich phases causes a corresponding nanoscale roughness.

Other researchers have also observed the change in roughness in chalcogenide photoresists due to etching.[36,37] Increase in the roughness in developed regions is due to the spatial variations in etching rate arising from nanostructurization in chalcogenides. However Dan'ko et al. have considered the case of photoinduced positive etching, i.e., the increased etching rate in areas that are exposed to light during etching. Koreshev and Ratushnyi[37] have also found an increase in roughness in unexposed developed films related to the nanostructural variations caused by initial cluster structure of the chalcogenide films. Their results related to exposed developed films is relevant to the minimization of roughness in lens arrays and will be discussed in the next section.

3.6. Minimization of Roughness in Lens Arrays. As discussed previously, rough surfaces cause adverse consequences for the focusing effect of the chalcogenides lenses and are thus undesirable for optical applications. Thus, a good patterning technique for chalcogenide lens arrays should result in relatively smooth and curved surfaces. Figure 7A and B show optical profilometer scans of the lens arrays exposed for 900 and 1800 s, respectively. The profile of these lenses was fitted to a smooth function to calculate the roughness in a lens pattern. The roughness of lenses patterned at 900 and 1800 s exposure time was 1.0 ± 0.5 nm and 14 ± 1 nm, respectively. The 3D profile of the 900 s exposed lens array clearly illustrates that the lenses are smoother with less defects compared to the lenses patterned at the 1800 s exposure time. It is to be noted that the roughness or deviation from smooth structures in the case of the 900 s exposure is different from the roughness measured for blank exposed films. This may be due to the lower exposure intensity at grayscale values lower than white in the lens structures resulting in a lower local exposure dose. However, if only this effect is considered, the roughness of the 1800 s exposed lens arrays would have also decreased. This not

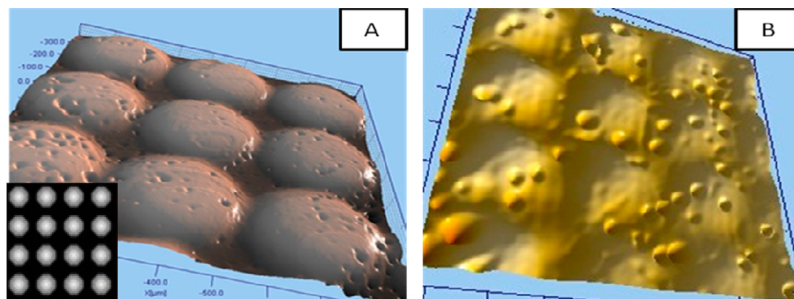

Figure 7. Optical profilometer image of lens with (A) 900 s exposure time and (B) 1800 s exposure time. Inset in panel (A) shows the grayscale digital mask used.

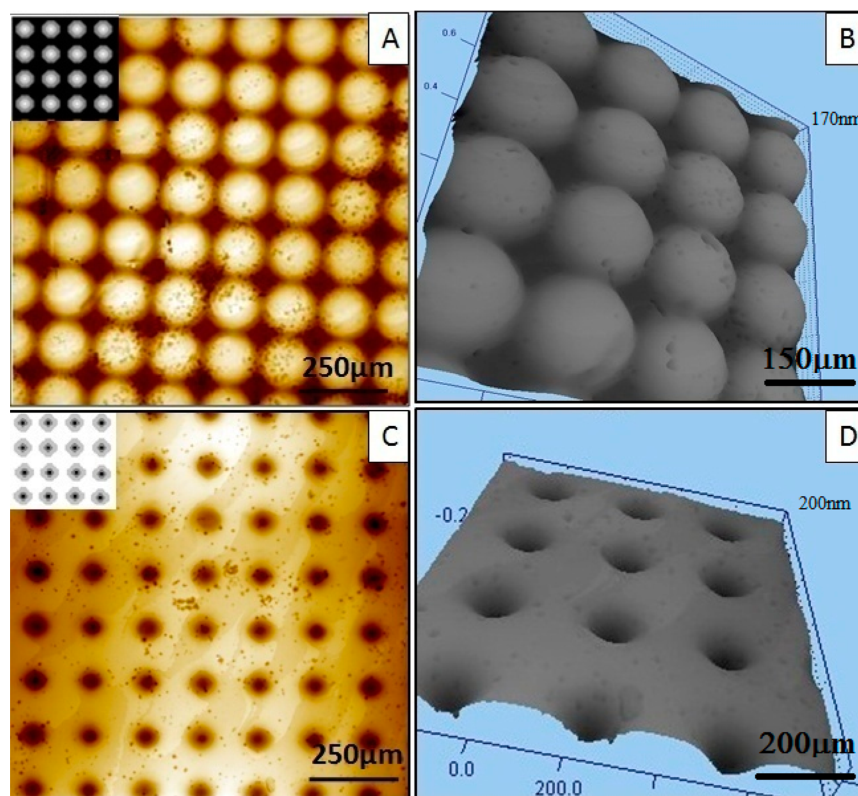

Figure 8. Optical profilometer image of (A) convex microlens arrays and their (B) 3D view. (C) Concave microlens arrays and their (D) 3D view (insets in panels (A) and (C) show the grayscale mask used).

being the case, it is possible that the surface distribution of nanophases does not increase linearly in this range of exposure dose.

In this context, the work by Koreshev and Ratushnyi[37] reveals that the roughness of films exposed to form relief phase holograms using energies up to 200 mJ/cm^2 lies between the roughness of unexposed developed films and unexposed undeveloped films. This is because of a decrease in the nanostructurization. This is contrary to our observed trend of roughness in films at blank (white) exposure times between 900 and 3600 s, i.e., exposure dose between 3150 and 12600 mJ/cm^2. However, it can serve to explain the observed difference in roughness between grayscale-patterned lens arrays and blank exposure films. At grayscale values below 255, the lower exposure dose might lead to a phase distribution of a much lower length scale than at higher exposure doses, thus resulting in a lower roughness than expected from the roughness trend at higher exposure doses. A further understanding of the chemical changes that occur on exposure to UV light at different exposure doses is required in order to optimize both roughness and lens height.

3.7. Patterning of Lens Arrays: Fabrication of Convex and Concave Lenses. Having optimized the grayscale lithography parameters (developer, ethanolamine; developing time, 3 min; exposure time, 900s), we attempted the fabrication of chalcogenide lens arrays. From an application point of view, both concave and convex structures are important. Concave structures can act as waveguides, and convex lenses can focus light in the IR region. By using a negative of the mask (substituting grayscale value x by $255 - x$), we were able to fabricate both structures as shown in Figure 8. The 3D profiles obtained from optical profilometer are shown on the right and illustrate a relatively smooth profile for both concave and convex lenses.

3.8. Focal Length of Lenses. The dimensions and profile of the convex lens array were used to calculate the effective focal length. The focal length of the spherical lenses can be calculated using the following equation[38]

$$F = \frac{h^2 + \left(\frac{d^2}{4}\right)}{2h(n - 1)}$$

where h represents the microlens thickness, d represents the diameter of the microlens, n represents the refractive index of the As_2Se_3 at 3 μm, which is 2.78. The dimension of the plano–convex lens was obtained from the optical profilometry graph shown in Figure 9. A plano–convex lens array with a very long focal length of ~9.3 mm with a surface roughness less than 5 nm could thus be fabricated using grayscale maskless lithography.

4. CONCLUSIONS

Maskless grayscale lithography and wet etching using ethanolamine have been successfully used for the fabrication of smooth 3D optical structures in amorphous As_2Se_3 films for IR optics applications. This is a direct and simple single lithographic step fabrication process that allows variation of thickness across a microlens array in a controllable reproducible manner. The exposure and etching parameters were optimized to result in smooth reproducible and periodic lens structures. Cylindrical lenses and concave and convex periodic arrays were fabricated with minimal roughness on an ~1 cm^2 area. The focal length of the plano–convex lens was calculated to be ~9.3 mm, establishing the utility of these lens arrays for optical focusing

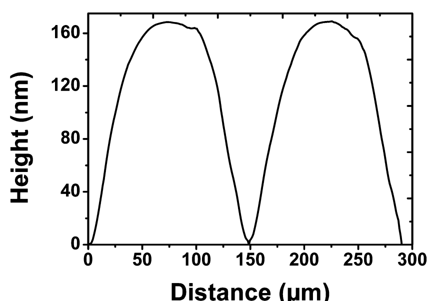

Figure 9. Profile of plano−convex lens having a 150 μm diameter and a 170 nm height as measured by optical profilometry.

applications in the IR region. It is to be noted that while we have demonstrated lens arrays having a single repeating pattern, it is possible to vary the dimensions and thickness, as well as the type of pattern across the array, by using the same method. The difference between roughness on a blank exposed As_2Se_3 film and the roughness of the lens patterned at the same exposure time of 900 s is an interesting observation that can potentially lead to better optimization of the exposure dose for smooth and tall structures.

AUTHOR INFORMATION

Corresponding Author

*E-mail: ashutos@iitk.ac.in.

Author Contributions

The manuscript was written by contributions of all authors. All authors have given approval for the final version of the manuscript.

Notes

The authors declare no competing financial interest.

ACKNOWLEDGMENTS

We acknowledge the support of the Department of Science and Technology (DST) to the Unit on Soft Nanofabrication at IIT Kanpur and Defense Research and Development Organization, New Delhi, India. We are thankful to Satinder Kumar Sharma, IIT Mandi for discussions.

REFERENCES

(1) Zakery, A.; Elliott, S. R. *J. Non-Cryst. Solids* **2003**, *330*, 1−12.
(2) Shimakawa, K.; Kolobov, A.; Elliott, S. R. *Adv. Phys.* **1995**, *44*, 475−588.
(3) DeCorby, R. G.; Ponnampalam, N.; Pai, M. M.; Nguyen, H. T.; Dwivedi, P. K.; Clement, T. J.; Haugen, C. J.; McMullin, J. N.; Kasap, S. O. *IEEE J. Sel. Top. Quantum Electron.* **2005**, *11*, 539−546.
(4) Klebanov, M.; Lyubin, V.; Kirzhner, M. G.; Abdulhalim, I. *J. Appl. Phys.* **2013**, *113*, 033503−6.
(5) Abdulhalim, I.; Gelbaor, M.; Klebanov, M.; Lyubin, V. *Opt. Mater. Express* **2011**, *1*, 1192−1201.
(6) Kaganovskii, Y.; Beke, D. L.; Kokenyesi, S. *Appl. Phys. Lett.* **2010**, *97*, 061906−3.
(7) Kovalskiy, A.; Vlcek, M.; Jain, H.; Fiserova, A.; Waits, C. M.; Dubey, M. *J. Non-Cryst. Solids* **2006**, *352*, 589−594.
(8) Tsiulyanu, D. *Non-Crystalline Materials for Optoelectronics*; Optoelectronic Materials and Devices Series; INOE Publishing House: Bucharest, Romania, 2004; Vol. 1, p 297.
(9) Vlcek, M.; Jain, H. *J. Optoelectron. Adv. Mater* **2006**, *8*, 2108−2111.
(10) Bryce, R. M.; Nguyen, H. T.; Nakeeran, P.; DeCorby, R. G.; Dwivedi, P. K.; Haugen, C. J.; McMullin, J. N.; Kasap, S. O. *J. Vac. Sci. Technol., A* **2004**, *22*, 1044−1047.
(11) Bureau, B.; Zhang, X. H.; Smektala, F.; Adam, J.-L.; Troles, J.; Ma, H.-l.; Boussard-Plèdel, C.; Lucas, J.; Lucas, P.; Le Coq, D.; Riley, M. R.; Simmons, J. H. *J. Non-Cryst. Solids* **2004**, *345*−*346*, 276−283.
(12) van Popta, A.; DeCorby, R.; Haugen, C.; Robinson, T.; McMullin, J.; Tonchev, D.; Kasap, S. *Opt. Express* **2002**, *10*, 639−644.
(13) Shankar, M.; Willett, R.; Pitsianis, N.; Schulz, T.; Gibbons, R.; Te Kolste, R.; Carriere, J.; Chen, C.; Prather, D.; Brady, D. *Appl. Opt.* **2008**, *47*, B1−B10.
(14) Kovalskiy, A.; Cech, J.; Vlcek, M.; Waits, C. M.; Dubey, M.; Heffner, W. R.; Jain, H. *J. Micro/Nanolithogr., MEMS, MOEMS* **2009**, *8*, 043012−043012.
(15) Eisenberg, N.; Manevich, M.; Arsh, A.; Klebanov, M.; Lyubin, V. *J. Optoelectron. Adv. Mater* **2002**, *4*, 405−407.
(16) Eisenberg, N.; Klebanov, M.; Lyubin, V.; Manevich, M.; Noach, S. *J. Optoelectron. Adv. Mater.* **2000**, *2*, 147−152.
(17) Manevich, M.; Klebanov, M.; Lyubin, V.; Varshal, J.; Broder, J.; Eisenberg, N. *Chalcogenide Lett.* **2008**, *5*, 58−60.
(18) Manevich, M.; Klebanov, M.; Lyubin, V.; Varshal, J.; Border, J.; Eisenberg, N. *Chalcogenide Lett.* **2008**, *5*, 61−64.
(19) Eisenberg, N.; Manevich, M.; Arsha, A.; Klebanova, M.; Lyubina, V. *Chalcogenide Lett.* **2005**, *2*, 35−37.
(20) Orava, J.; Kohoutek, T.; Greer, A. L.; Fudouzi, H. *Opt. Mater. Express* **2011**, *1*, 796−802.
(21) Bulanovs, A.; Gerbreders, V.; Kirilovs, G.; Teteris, J. *Cent. Eur. J. Phys.* **2011**, *9*, 1327−1333.
(22) Dan'ko, V. A.; Indutnyi, I. Z.; Min'ko, V. I.; Shepelyavyi, P. E. *Optoelectron., Instrum., Data Process.* **2010**, *46*, 483−490.
(23) Dan'ko, V. A.; Indutnyi, I. Z.; Min'ko, V. I.; Shepelyavyi, P. E.; Bereznyova, O. V.; Lytvyn, O. S. *Semiconductors* **2012**, *46*, 504−508.
(24) Rammohan, A.; Dwivedi, P. K.; Martinez-Duarte, R.; Katepalli, H.; Madou, M. J.; Sharma, A. *Sens. Actuators, B* **2011**, *153*, 125−134.
(25) Němec, P.; Frumar, M.; Jedelský, J.; Jelínek, M.; Lančok, J.; Gregora, I. *J. Non-Cryst. Solids* **2002**, *299*, 1013−1017.
(26) Dwivedi, P. K.; Sharma, S. K.; Rammohan, A.; Sharma, A. *AIP Conf. Proc.* **2011**, *1349*, 555−556.
(27) Antoine, K.; Jain, H.; Vlcek, M. *J. Non-Cryst. Solids* **2006**, *352*, 595−600.
(28) Tanaka, K.; Saitoh, A.; Terakado, N. *J. Optoelectron. Adv. Mater.* **2006**, *8*, 2058−2065.
(29) Ramachandran, S.; Pepper, J. C.; Brady, D. J.; Bishop, S. G. *J. Lightwave Technol.* **1997**, *15*, 1371−1377.
(30) Carlie, N. A. A Solution-Based Approach to the Fabrication of Novel Chalcogenide Glass Materials and Structures. Ph.D. Thesis, Clemson University, March 2010.
(31) Mamedov, S.; Mikhailov, M. *J. Non-Cryst. Solids* **1997**, *221*, 181−186.
(32) Michailov, M. D.; Mamedov, S. B.; Tsventarnyi, S. V. *J. Non-Cryst. Solids* **1994**, *176*, 258−262.
(33) Eggleton, B. J.; Luther-Davies, B.; Richardson, K. *Nat. Photonics* **2011**, *5*, 141−148.
(34) Sanchez, E. A.; Waldmann, M.; Arnold, C. B. *Appl. Opt.* **2011**, *50*, 1974−1978.
(35) Choi, D.-Y.; Madden, S.; Rode, A.; Wang, R.; Bulla, D.; Luther-Davies, B. *J. Non-Cryst. Solids* **2008**, *354*, 5253−5254.
(36) Dan'ko, V.; Indutny, I.; Myn'ko, V.; Shepeliavyi, P.; Lykanyuk, M.; Lytvyn, O. *J. Non-Oxide Glasses* **2012**, *3*, 13−18.
(37) Koreshev, S. N.; Ratushnyĭ, V. P. *Opt. Spectrosc.* **2009**, *106*, 288−292.
(38) Savastru, D.; Miclos, S.; Savastru, R. *J. Optoelectron. Adv. Mater.* **2005**, *7*, 1909−1913.